PERFORMANCE OF EQUIVALENT FORCE CONTROL METHOD FOR REAL-TIME SUBSTRUCTURE TESTING

B. Wu[1], G.S. Xu[2], Y. Li[3], P.B. Shing[4] and J.P. Ou[5]

[1] *Professor, School of Civil Engineering, Harbin Institute of Technology, Harbin 150090, China*
Tel.: 0086-451-86283765. Fax: 0086-451-86282704. E-mail: bin.wu@hit.edu.cn
[2] *Doctoral student, School of Civil Engineering, Harbin Institute of Technology, Harbin 150090, China*
[3] *Lecturer, School of Oil Gas Engineering, China University of Petroleum, Beijing 102249, China*
[4] *Professor, Department of Structural Engineering, University of California at San Diego, CA 92093-0085, USA*
[5] *Professor, Dalian University of Technology, Dalian 116024, China; School of Civil Engineering, Harbin Institute of Technology, Harbin 150090, China*

ABSTRACT :

The equivalent force control (EFC) method has been developed for real-time substructure testing (RSTing) with implicit integration to replace the numerical iterative process with a feedback control. This paper addresses two issues concerning the performance of this method. One is the determination of the force-displacement conversion factor (a key component of EFC) for nonlinear specimens. The analysis conducted here shows that the force-displacement conversion factor is largely governed by the mass and damping properties of the numerical substructure and the properties of the numerical scheme when a small integration time interval is used. Otherwise, the factor has to be determined with the secant stiffness of the specimen and of the numerical substructure if a PD controller is used for EFC. The other issue is the overshooting problem which may arise for multi-degree-of-freedom structures due to the relatively quick response feedback from the numerical substructure in the closed-loop EFC. It is shown that this problem can be resolved by reducing either the EFC gains or the increment size of the equivalent force command. The analytical studies on these two issues are verified by RSTs conducted on structural models with buckling restrained braces and an offshore platform with Magnetorheological dampers.

KEYWORDS: real-time substructure test, hybrid simulation, equivalent force control, implicit integration, pseudodynamic test

1. INTRODUCTION

Real-time substructure testing (RSTing) is a hybrid simulation technique, in which a structure is split into an experimental test specimen and a numerical model, and the dynamic behavior of the entire structure is simulated in real-time. Since it was presented in the 1990s (Nakashima et al. 1992), RSTing has been used and advanced by researchers worldwide, and has been developed rapidly in terms of step-by-step time integration schemes (Wu et al. 2006; Jung et al. 2007), estimation and remedy of real-time errors such as time delay and its compensation (Mercan and James 2007; Spencer and Carrion 2007), actuation control methods(Shao and Reinhorn 2006; Bonnet et al. 2007; Lim et al. 2007), and applications to theoretical and practical problems (Wallace et al. 2007).

A key element of the RSTing is the numerical algorithm that is used to perform the stepwise integration of the equations of motion. Numerical integration algorithms are divided into explicit and implicit types. A disadvantage for most of the explicit algorithms is the conditional stability. Many implicit algorithms are unconditionally stable, but they normally need time consuming iteration to solve the nonlinear equations of motion.

To avoid the numerical iteration process associated with implicit integration, Wu et al. (2007) have proposed a new method for general hybrid simulation. This is called the equivalent force control (EFC) method. The specific advantage of the EFC method is that it transforms the problem of solving an implicit equation into a

standard feedback tracking problem with an explicit reference input and a plant (which is represented by the combined physical and numerical substructures) to be controlled. Although the method has been validated with numerical simulations and actual tests (Wu et al. 2007), this paper focuses on two critical issues that affect its performance. One is the force-displacement conversion factor for nonlinear specimens, and the other is the overshooting problem which may arise for multi-degree-of-freedom structures (MDOF). Methods to overcome these issues are proposed and validated with actual tests of structures with Buckling-Restrained Braces and an offshore platform (identified as JZ20-2NW) with Magnetorheological (MR) dampers.

2. OVERVIEW OF EFC METHOD

With the Newmark constant-average-acceleration (CAA) method, the time-discretized equations of motion for a RST and the acceleration and velocity approximations at step i+1 are expressed as

$$\mathbf{M}_{\mathrm{N}}\mathbf{a}_{i+1}+\mathbf{C}_{\mathrm{N}}\mathbf{v}_{i+1}+\mathbf{R}_{\mathrm{N}}(\mathbf{d}_{i+1})+\mathbf{R}_{\mathrm{E}}(\mathbf{a}_{i+1},\mathbf{v}_{i+1},\mathbf{d}_{i+1})=\mathbf{F}_{i+1} \tag{2.1}$$

$$\mathbf{a}_{i+1}=\frac{4}{\Delta t^2}(-\mathbf{d}_i-\Delta t\mathbf{v}_i-\frac{\Delta t^2}{4}\mathbf{a}_i+\mathbf{d}_{i+1}) \tag{2.2}$$

$$\mathbf{v}_{i+1}=-\frac{2}{\Delta t}\mathbf{d}_i-\mathbf{v}_i+\frac{2}{\Delta t}\mathbf{d}_{i+1} \tag{2.3}$$

where **d**, **v**, and **a** are the displacement, velocity, and acceleration vectors; $\mathbf{M}_{\mathrm{N}}$, $\mathbf{C}_{\mathrm{N}}$, $\mathbf{R}_{\mathrm{N}}$ are the mass, damping, and static restoring force vectors of the numerical substructure; $\mathbf{R}_{\mathrm{E}}$ is the restoring force vector of the experimental substructure including static, damping, and inertia forces; **F** is the external excitation force vector; and Δt is the integration time interval. Substituting Eqn. 2.2 and 2.3 into 2.1 gives

$$\mathbf{R}_{\mathrm{N}}(\mathbf{d}_{i+1})+\mathbf{K}_{\mathrm{PD}}\mathbf{d}_{i+1}+\mathbf{R}_{\mathrm{E}}(\mathbf{a}_{i+1},\mathbf{v}_{i+1},\mathbf{d}_{i+1})=\mathbf{F}_{\mathrm{EQ},i+1} \tag{2.4}$$

where

$$\mathbf{K}_{\mathrm{PD}}=\frac{4\mathbf{M}_{\mathrm{N}}}{\Delta t^2}+\frac{2\mathbf{C}_{\mathrm{N}}}{\Delta t} \tag{2.5}$$

$$\mathbf{F}_{\mathrm{EQ},i+1}=\mathbf{F}_{i+1}+\mathbf{M}_{\mathrm{N}}\mathbf{a}_i+(\frac{4\mathbf{M}_{\mathrm{N}}}{\Delta t}+\mathbf{C}_{\mathrm{N}})\mathbf{v}_i+(\frac{4\mathbf{M}_{\mathrm{N}}}{\Delta t^2}+\frac{2\mathbf{C}_{\mathrm{N}}}{\Delta t})\mathbf{d}_i \tag{2.6}$$

in which $\mathbf{K}_{\mathrm{PD}}$ is called the pseudodynamic stiffness, and $\mathbf{F}_{\mathrm{EQ}}$ the equivalent force. The solution of Eqn. 2.4 can be interpreted as finding the response of a hybrid system, which consists of numerical and experimental substructures with real and pseudodynamic forces, to an explicit equivalent load. This response can be obtained by directly applying the equivalent force to the hybrid system, in which the numerical substructure and pseudodynamic forces are evaluated in a computer, using a force-feedback control strategy. When the damping and inertia effects in $\mathbf{R}_{\mathrm{E}}$ are insignificant, the EFC method becomes a quasi-static pseudodynamic test method.

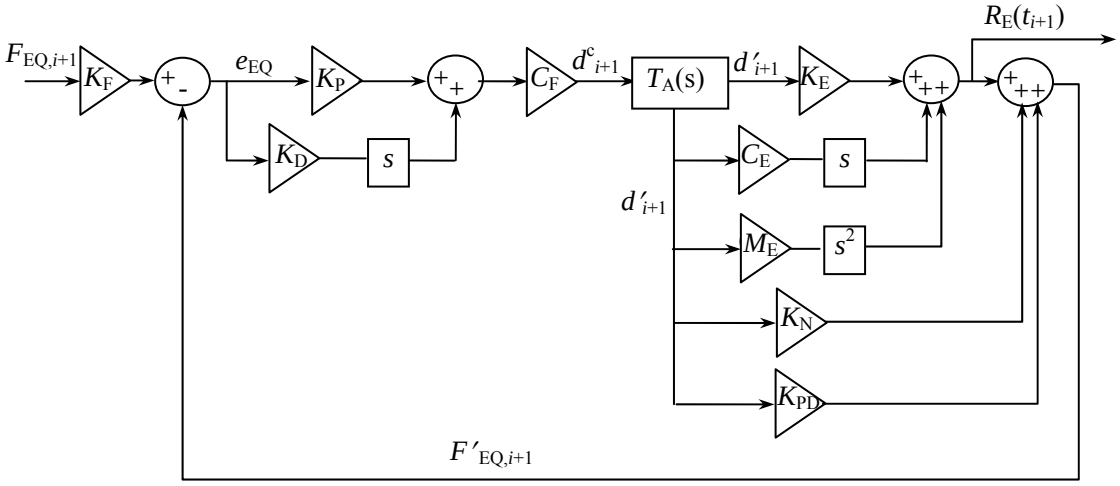

Figure 1. Block diagram of EFC method.

The block diagram representing an EFC system for a linear single-degree-of-freedom (SDOF) structure is shown in Fig. 1, in which K_N and K_E are the stiffness of the numerical and experimental substructures, respectively, $\boldsymbol{C}_E$ is the damping coefficient of the experimental substructure, and $\boldsymbol{T}_A(s)$ is the transfer function of the actuator including a displacement-feedback controller. The equivalent force controller shown in Figure 1 is a proportional-derivative (PD) controller, in which K_P and K_D are the proportional and derivative gains, respectively. The factor K_F after the equivalent force command $F_{EQ,i+1}$ is used to eliminate the steady-state error of the PD controller. After being processed by a force controller, the force error e_{EQ} between the equivalent force command modified by K_F and the equivalent force feedback $F'_{EQ,i+1}$ is converted to a displacement command d^c_{i+1} by a conversion factor C_F. Then the actuator is controlled with a displacement control mode. The terms R_E and d'_{i+1} are the reaction force and the displacement response of the experimental substructure subjected to the command d^c_{i+1}. At the end of the $(i+1)$th step, the reaction force $R_E(t_{i+1})$ is fed back to the computer to calculate the displacement, velocity and acceleration responses of the structure at the end of the time step using Eqn. 2.1-2.4.

3. FORCE-DISPLACEMENT CONVERSION FACTOR FOR NONLINEAR STRUCTURES

Comparing the EFC method with mathematical iteration, one may find that the force-displacement conversion factor is equivalent to the Jacobian factor used in the Newton iteration method. It is therefore advised in Wu et al. (2007) that the factor C_F can be taken as a constant and be constructed with the partial derivatives of the left-hand side of Eqn. 2.4 with respective to d_{i+1} at the initial state of the test structure, similar to a modified Newton method. For an EFC system with a linear test structure as shown in Fig. 1, it has been proved in Wu et al.(2007) that zero steady-state control error can be achieved if

$$C_F = (K_N + K_{PD} + K_E)^{-1} \tag{3.1}$$

$$K_F = (1 + K_P)/K_P \tag{3.2}$$

Note that Eqn. 3.1 holds only for a specimen whose damping and inertia forces are insignificant. Otherwise, the expression for C_F should contain the damping and/or inertia properties.

Next, we discuss the formulation of C_F for nonlinear test structures with negligible inertia and damping effects. Focusing on the effect of C_F, we assume an ideal actuator with its transfer function equal to unity. For such a case, it can be shown that the equivalent force feedback can be expressed as follows.

$$F'_{EQ,i+1} = K_{PD}C_F[K_P(K_F F_{EQ,i+1} - F'_{EQ,i+1}) + K_D(K_F \dot{F}_{EQ,i+1} - \dot{F}'_{EQ,i+1})] + R_N + R_E \tag{3.3}$$

For a small K_D, the above equation can be approximated by

$$F'_{EQ,i+1} = K_{PD}C_F K_P(K_F F_{EQ,i+1} - F'_{EQ,i+1}) + R_N + R_E \tag{3.4}$$

If the inertia and damping effects of the experimental specimen are ignored, we can define a secant stiffness of the entire structure as

$$K_S = \frac{R_N(d'_{i+1}) + R_E(d'_{i+1})}{d'_{i+1}} \tag{3.5}$$

When the actuator dynamics is ignored, one has

$$d'_{i+1} = C_F K_P(K_F F_{EQ,i+1} - F'_{EQ,i+1}) \tag{3.6}$$

With Eqn. 3.4, 3.5 and 3.6, one can solve for $F'_{EQ,i+1}$ as

$$F'_{EQ,i+1} = \frac{K_F K_P C_F(K_{PD} + K_S)}{1 + K_P C_F(K_{PD} + K_S)} F_{EQ,i+1} \tag{3.7}$$

From Eqn. 3.7, we see that the coefficient term of $F_{EQ,i+1}$must be equal to one in order to achieve zero error in EFC. To achieve this with Eqn. 3.2, one must have

$$C_F = (K_{PD} + K_S)^{-1} \tag{3.8}$$

It is seen from the above equation that C_F needs to depend on K_S, which may vary from one time step to the next for a nonlinear experimental substructure, if no equivalent force error is desired.

However, from Eqn. 3.8, one can see that the variation of C_F with respect to K_S is insignificant when $K_{PD} >> K_S$.

With Eqn. 2.5 and by ignoring C_N, one can easily see that $K_{PD} >> K_S$ when

$$(\omega_S \Delta t)^2 \ll 4 \tag{3.9}$$

where $\omega_S = \sqrt{K_S / M_N}$. For MDOF structures, the above condition can be evaluated in the modal space using a secant stiffness matrix. Hence, when Inequality 3.9 is satisfied, K_S can simply take the value of initial stiffness of the structure. It is interesting to note that Inequality 3.9 is identical to the stability condition of the central difference method with zero damping. However, it is important to point out that for the EFC, this condition only applies to the dominant frequency in the response rather than the highest frequency of the structure. A similar condition as Inequality 3.9 can be obtained for cases where the damping and inertia forces of the specimen are important. When Inequality 3.9 is not satisfied, i.e., when $(\omega_S \Delta t)^2$ is close to 4 or larger, a good estimate of the secant stiffness is necessary. For this purpose, one can predict the secant stiffness of the experimental structure at the end of the time step based on the measured reaction forces and displacements provided that the stiffness of a specimen does not change drastically over a small time interval. When the secant stiffness of a structure cannot be accurately assessed, the equivalent force controller needs to be improved to minimize the control errors. One such possibility is to add an integral gain to the controller.

4. OVERSHOOTING PROBLEM FOR MDOF STRUCTURES

In general, the configuration of the block diagram for an EFC test of a MDOF structure may be different from that shown in Fig. 1 for a SDOF structure. As discussed in Wu et al.(2007), for a MDOF structure, the input to the numerical part, including the numerical substructure and pseudo-dynamic stiffness, can be a direct displacement command while that to the experimental substructure is the output of an actuator. This is because it is quite possible that numerical and experimental substructures do not share the same degrees of freedom. As a result, they do not share the same inputs. Without the actuator dynamics, the response of a numerical substructure to an input signal is almost instantaneous except for a very small time delay required for the computation of the response. This causes what is referred to here as an overshoot problem and will alter the dynamics of the entire hybrid system.

To illustrate the overshoot problem in a simple manner, we consider the RST of a SDOF structure, for which the displacement command d^c_{i+1} is imposed directly on the numerical substructure which includes the static stiffness K_N and the pseudodynamic stiffness K_{PD}, but the displacement command to the experimental part is through an actuator, as opposed to what is shown in Fig. 1. When $K_{PD} >> K_E$ and by ignoring the damping C_E and mass M_E and considering only the proportional control, the equivalent force response to a step input at the jth sampling instant is

$$F'^{j}_{EQ,i+1} = F_{EQ,i} + \Delta F_{EQ,i+1} K_F K_{PFV} \frac{1-(-K_{PFV})^j}{1+K_{PFV}} \tag{4.1}$$

in which

$$K_{PFV} = K_P C_F (K_{PD} + K_N), \qquad \Delta F_{EQ,i+1} = F_{EQ,i+1} - F_{EQ,i} \tag{4.2}$$

Eqn. 4.1 shows that the equivalent force response will oscillate as a function of the sampling points j. Assuming that K_P is sufficiently small so that $K_{PFV}<1$, the maximum value of equivalent force response can be obtained by having $j = 1$ as

$$F'^{\max}_{EQ,i+1} = F_{EQ,i+1} + K_P \Delta F_{EQ,i+1} \tag{4.3}$$

From the above equation, we see that the overshooting of the equivalent force response is approximately equal to $K_P \Delta F_{EQ,i+1}$ if $K_{PD} >> K_E$.

According to Fig. 1, when K_{PD} is dominant, the displacement command is obtained as

$$d^c_{i+1} = F'^{j}_{EQ,i+1} / K_{PD} \tag{4.4}$$

Hence, the displacement command contains the same features of overshooting and oscillation as the effective force response. This causes two negative consequences. For a test specimen that has a hysteretic behavior, these force the specimen through an unrealistic displacement history and will thereby result in an inaccurate response.

From the actuator control point of view, the oscillation may destabilize the control. Hence, these problems need to be resolved.

It is seen from Eqn. 4.1 and 4.3 that the overshoot and oscillation of the equivalent force response are related to the control gain K_P and the equivalent force command increment. Therefore, a straightforward way to reduce equivalent force overshoot as well as oscillation is to lower the values of either K_P or $\Delta F_{EQ,i+1}$ or both. The equivalent force command increment can be reduced by interpolation between the integration time instants. This is proven to be effective in the tests presented below.

5. EXPERIMENTAL STUDY WITH BUCKLING-RESTRAINED BRACE SPECIMEN

The schematic of the SDOF test structure is shown in Fig. 2. The parameters of the numerical substructure are: M_N=6×10^6 kg, K_N=1.2×10^8 N/m, and C_N=3.79×10^6 N·s/m. The integration time interval is 0.01s. With the above parameters, the pseudo-dynamic stiffness was obtained from Eqn. 2.5 as 2.408×10^{11} N/m. The experimental substructures were steel buckling-restrained braces (BRBs). The length of the core plate of the braces was 1180 mm. The brace had a cruciform core as shown in Fig. 3. The steel plates were Grade Q235, whose Young's modulus was 2×10^5 MPa and nominal yield strength was 235MPa. The BRBs were loaded with the same MTS servo-hydraulic actuator as in the spring tests. A photograph of the experimental setup is shown in Fig. 4. Experimental tests were conducted at the Mechanical and Structural Testing Center of the Harbin Institute of Technology

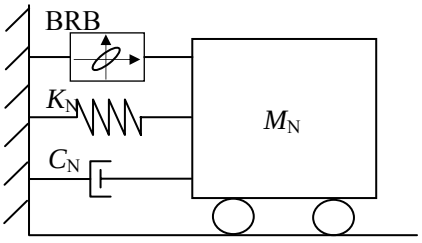

Figure 2. Schematic of SDOF test structure with BRB specimen

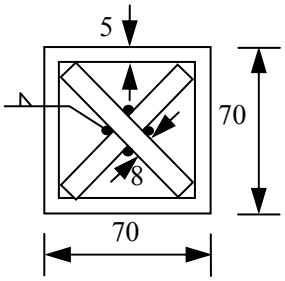

Figure 3. Cross section of BRBs for test

Figure 4. Photograph of experimental setup with BRB specimen

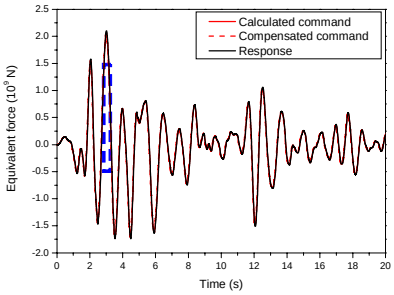

Figure 5(a). Equivalent force commands and responses of RST with BRB specimen (overall view)

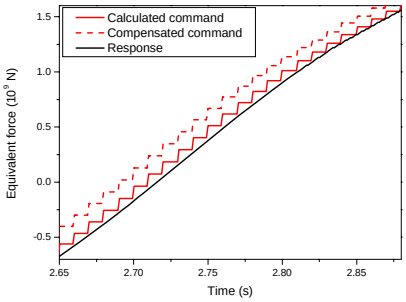

Figure 5(b). Equivalent force commands and responses of RST with BRB specimen (close-up view)

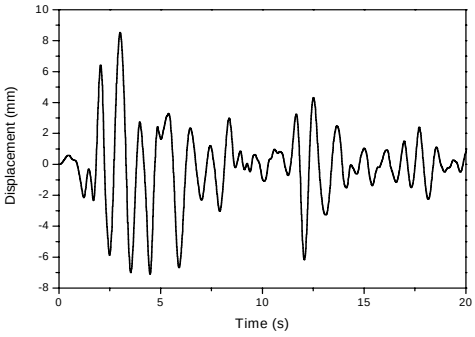

Figure 6(a). Displacement response of BRB from the RST

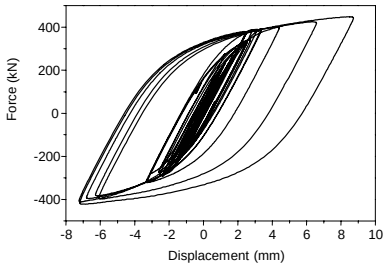

Figure 6(b). Hysteretic loop of the BRB

The calculated initial stiffness of the brace was 1.5×10^8 N/m. The period of the test structure was obtained as 0.9366 s. Preliminary tests had shown that the equivalent force responses had a dynamic time delay of about 0.028 s (Li, 2007). A modified version of the third order polynomial extrapolation method proposed by Horiuchi et al. (1999) was used to compensate for the delay.

The secant stiffness of the BRB specimen at the previous integration time step was used to calculate the force-displacement conversion factor. The excitation used was again the El Centro (NS, 1940) ground motion but with a peak acceleration of 0.4 m/s^2. The equivalent force response with the delay compensation is shown in Fig. 5, where the effectiveness of the compensation can be observed. The good tracking performance of the effective force command implies that the result of the RST is accurate. The displacement response and the corresponding hysteretic loops from the test are shown in Fig. 6.

6. APPLICATION OF EFC METHOD TO AN OFFSHORE PLATFORM

To suppress the vibration mainly induced by ice and earthquake loads, an isolation layer was designed between the main deck and top of the supporting jacket of the JZ20-2NW offshore platform located in Bohai Gulf of China. A photo of the platform is shown in Fig. 7. The detail of the isolation layer is shown in Fig. 8. It comprised 8 rubber isolators and 8 Magnetorheological (MR) dampers. The isolators were placed at the four corners and the center area of the isolation layer. The dampers were incorporated around the corners of the isolation layer. The entire structure was simplified into an 8-degree-of-fredoom (8DOF) model as shown in Fig. 9. The structural parameters except for MR dampers can be found in Wang et al. (2006).

An MR damper which had zero drive voltage to act as a passive fluid viscous damper was the experimental substructure and the remainder of the structure was the numerical substructure. The testing setup is shown in Fig. 10. Both the EFC method and the CDM with conventional displacement control were considered in this study. The tests were performed using the same experimental facility as in the previous section of this paper.

Figure 7. Photo of JZ20-2NW offshore platform

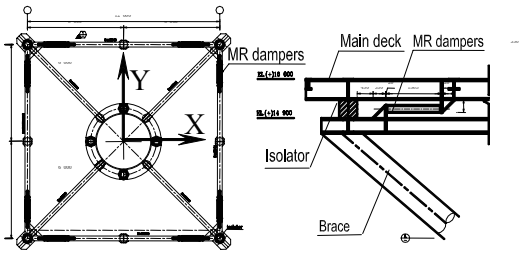

Figure 8. Isolation layer of JZ20-2NW platform

The equivalent force command calculated with Eqn. 2.6 in each integration time step was divided into 20

sub-steps using linear interpolation in order to smooth the velocity response. The earthquake inputs were the El Centro (NS, 1940) and Taft (N21E, 1952) ground motions with peak acceleration of 1.00 m / s^2, and the Tianjin (1976) record with peak acceleration of 0.35 m / s^2. The control gains of the equivalent force controller were K_P = 0.5 and K_D = 0. The integration time interval in the tests was chosen to be 0.02s.

The experimental drifts of the isolation layer subject to the El Centro (NS, 1940) record are shown in Fig. 11. It is seen that the response of the RST using the CDM diverges, while that with the EFC method remains stable. The pure numerical result without dampers is also shown in Fig. 11, where the significant response mitigation effect of the dampers is observed. Fig. 12 shows the equivalent force response of the main deck. It is seen that the equivalent force response tracks the equivalent force command perfectly, which indicates that the test results obtained from the EFC method are accurate. Similar conclusions can be obtained from the tests using the Taft (N21E, 1952) and Tianjin (1976) records.

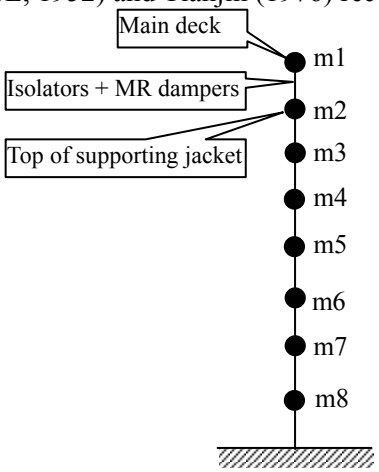

Figure 9. 8DOF model of the JZ20-2NW offshore platform

Figure 10. Testing setup for experimental substructure

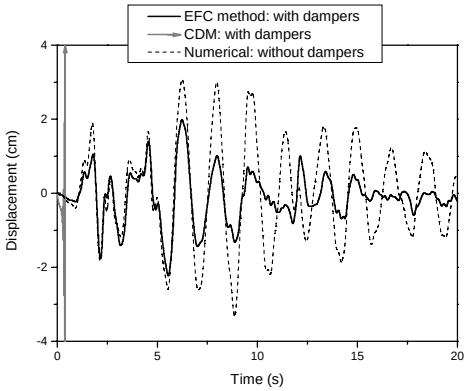

Figure 11. Drifts of the isolation layer

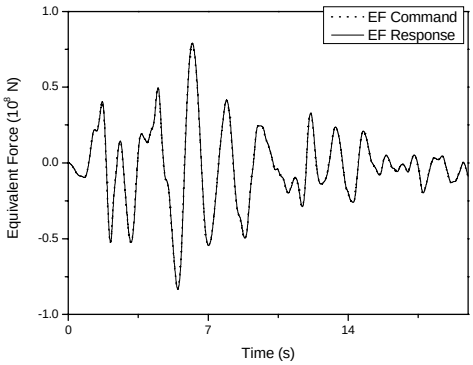

Figure 12. Equivalent force response of the main deck layer

7. CONCLUSIONS

This paper discusses two issues affecting the performance of the EFC method for real-time substructure tests and presents two actual tests with the method. The main conclusions are as follows.

(1) The force-displacement conversion factor C_F is one of the key components in EFC. For EFC with a PD controller, the proper selection of C_F requires the estimation of the secant stiffness (and damping) of the experimental and numerical substructures when these quantities are relatively large as compared to the pseudodynamic stiffness of the numerical substructure.

(2) An overshooting problem may occur in EFC for MDOF structures due to too quick a response of the numerical substructure in the closed loop of EFC. This can be resolved simply by reducing the EFC gains or using small subincrements of the equivalent force command. The excellent stability of the EFC method as compared to the CDM is experimentally verified by the RST of the JZ20-2NW offshore platform with MR dampers.

ACKNOWLEDGEMENTS

This work was supported by Grant 90715036 and 50578047 from the National Science Foundation of China，and China Ministry of Education through Program for New Century Excellent Talents in University. Mr. Y. Ma of the Mechanical and Structural Testing Center, Harbin Institute of Technology, is gratefully acknowledged for his assistance with the operation of the MTS testing system.

REFERENCES

Bonnet, P. A., Lim, C. N., Williams, M. S., Blakeborough, A., Neild, S. A., Stoten, D. P., and Taylor, C. A. (2007). Real-time hybrid experiments with Newmark integration, MCSmd outer-loop control and multi-tasking strategies. *Earthquake Engineering and Structural Dynamics* **36**, 119-141.

Horiuchi, T., Inoue, M., Konno, T., and Namita, Y. (1999). Real-time hybrid experimental system with actuator delay compensation and its application to a piping system with energy absorber. *Earthquake Engineering and Structural Dynamics* **28**, 1121-1141.

Jung, R.Y., Shing, P. B., Stauffer, E., and Thoen, B. (2007). Performance of a real-time pseudo dynamic test system considering nonlinear structural response. *Earthquake Engineering and Structural Dynamics* **36**, 1785-1809.

Li, Y. (2007). Seismic performance of buckling-restrained braces and substructure testing methods. Doctoral Thesis, Harbin Institute of Technology, Harbin, China (in Chinese).

Lim, C. N., Neild, S. A., Stoten, D. P., Drury, D., and Taylor, C. A. (2007). Adaptive control strategy for dynamic substructuring tests. *Journal of Engineering Mechanics*(ASCE) **113:8**, 864-873.

Mercan, O., and James, M. R. (2007). Stability and accuracy analysis of outer loop dynamics in real-time pseudodynamic testing of SDOF systems. *Earthquake Engineering and Structural Dynamics* **36**, 1523-1543.

Nakashima, M., Kato, H., and Takaoka, E. (1992). Development of real-time pseudo dynamic testing. *Earthquake Engineering and Structural Dynamics* **21:1**, 79-92.

Shao, X., and Reinhorn, A. M. (2006). Force controlled actuators in hybrid testing. *The fourth World Conference on Structural Control and Monitoring, University of California*, San Diego, 11-13 July, Paper No.245.

Spencer, B. F., and Carrion, J. E. (2007). Real-time hybrid testing of semi-actively controlled structure with MR damper. *Proceedings of the second International Conference on Advances in Experimental Structural Engineering*, Shanghai, China, December 4-6, 49-64.

Wallace, M. I., Wagg, D. J., Neild, S. A., Bunniss, P., Lieven, N. A. J., and Crewe, A. J. (2007). Testing coupled rotor blade–lag damper vibration using real-time dynamic substructuring. *Journal of Sound and Vibration* **307**, 737-754.

Wang, Q.Y., Wu, B., Ou, J.P., Guan, X.C., and Shi, P.F. (2006). Real-time Substructure Test of JZ20-2NW Offshore Platform with Passive MR Dampers. *The Eighth US National Conference on Earthquake Engineering*, San Francisco, California.

Wu, B., Xu, G., Wang, Q., and Williams, M. (2006). Operator-splitting method for real-time substructure testing. *Earthquake Engineering and Structural Dynamics* **35**, 293-314.

Wu, B., Wang, Q. Y., Shing, P. B., and Ou, J. P. (2007). Equivalent force control method for generalized real-time substructure testing with implicit integration. *Earthquake Engineering and Structural Dynamics* **36**, 1127-1149.